Halo-substituted azobenzenes adsorbed at Ag(111) and Au(111) interfaces: Structures and optical properties

Zak E. Hughes,[1,*] Alexander Baev,[2] Paras N. Prasad,[2] and Tiffany R. Walsh[1,†]

[1]*Institute for Frontier Materials, Deakin University, Geelong VIC 3216, Australia*

[2]*Institute for Lasers, Photonics and Biophotonics and the Department of Chemistry, The University at Buffalo,*
The State University of New York, Buffalo, New York 14260, USA

The adsorption of azobenzene (AB), *ortho* fluoro-azobenzene (FAB) and *ortho* chlor-azobenzol (ClAB), in both the *cis* and *trans* isomers, at the Au(111) and Ag(111) surfaces is investigated using plane-wave density functional calculations with the revPBE-vdW-DF functional. The resulting adsorption energies and internal structures of AB adsorbed to both metal surfaces are in broad agreement with available experimental data. In the gas phase, FAB and ClAB feature a significant reduction in the energy difference between the two isomeric states, compared with AB. This relative reduction in the energy difference is still significant for the adsorbed form of FAB but is only weakly apparent for ClAB. The absorption spectra of the molecules have also been calculated, with the halogen substituents generating significant changes in the gas phase, but only a modest difference for the adsorbed molecules.

I. INTRODUCTION

A major current focus in nanotechnology is the development of reversible bistable molecular and supramolecular switches that can undergo structural change following the application of an external stimulus [1–3]. Photoswitchable materials, i.e., materials that can change their molecular structure upon exposure to light, have significant potential applications including data storage [4] and actuating devices [5,6]. One of the most widely exploited molecular photoswitches is azobenzene (AB), which undergoes a *trans*-to-*cis* isomerization upon photoexcitation with UV light, with the reverse *cis*-to-*trans* conversion proceeding upon exposure to blue light. Incorporation of AB into a larger biomolecular structure offers opportunities to control specific biological targets *in vivo*, allowing optically controlled drug release [7,8], as well as in the field of bionanocombinatorics, where biomolecular noncovalent recognition can be used to assemble ordered nanostructures capable of reconfiguration [9–12]. Given that many of these applications involve the interface of the photoswitch in contact with a solid surface, elucidation of the structure and properties of AB and its derivatives, adsorbed at material interfaces, is much needed.

Recently, synthetic efforts have shown successful modification of AB such that the photoisomerization can be be activated in the visible light range [13–15]. Of particular interest are AB-based compounds that can be photoswitched in the red, far-red, or near-infrared regions of the electromagnetic spectrum. Such compounds have the advantage of *in vivo* photoswitching capabilities, because these wavelengths of light are able to pass through mammalian soft tissue [7,14]. The switching wavelength of a modified AB molecule can be controlled by using different substituents at the *ortho*, *meta*, and *para* positions of the phenyl rings. The number and different combinations of substituent groups that are

synthetically possible to date have generated a diverse and expanding library of AB compounds with many different properties [7,8,15].

Even relatively simple substitutions of AB can lead to quite different structures and properties relative to those of the parent AB molecule. For example, the substitution of the *ortho* hydrogens by fluorine can move both the *trans* →*cis* and the *cis* → *trans* transitions into the visible range [15–17]. In addition, *ortho*-fluoro substituted ABs are known to overcome another limitation of unmodified AB, namely that of the overlap of the $n \rightarrow \pi^*$ bands of the two isomers, which typically leads to incomplete *cis* → *trans* photoisomerization. In contrast to the parent AB molecule, *ortho*-fluoro substituted ABs feature a clear separation between the $n \rightarrow \pi^*$ bands of the *trans* and *cis* isomers, and thus support higher levels of photoconversion. Finally, the *cis* form of tetra *ortho*-fluoroazobenzene has exceptional thermal stability, with a reported half-life of approximately 700 days at 25 °C [16,17]. Substitution with chlorine rather than fluorine redshifts the transitions, allowing the *trans* → *cis* transition to be made using red light [14]. In addition, the presence of the electron-withdrawing Cl atoms results in modified ABs that show no photobleaching and are resistant to reduction by glutathione, both of which are desirable properties for photoswitchable compounds to be used *in vivo* [7,8,14]. Despite the many advantages of such substituted ABs, investigation of their structures are limited and have tended to concentrate on the gas phase [17–19]. However, to exploit these compounds to their fullest potential, a deeper comprehension of their structures and properties when adsorbed at material interfaces is needed.

Several previous studies have investigated the adsorption of AB on the (111) plane of noble-metal surfaces [20–27]. The experimentally determined adsorption energy of AB to the Au(111) and Ag(111) surfaces has been obtained *via* temperature programmed desorption (TPD) measurements [23,28], while the normal incidence x-ray standing-wave technique (NIXSW) has been used to provide information about the adsorbed geometry of the AB molecule [23–25]. Despite these studies, obtaining molecular-level details of

---

*[*]zhughes@deakin.edu.au

[†]tiffany.walsh@deakin.edu.au

the adsorbed structure of AB at noble-metal surfaces is challenging for experiment alone to address. To complement these experimental efforts, several theoretical studies have been reported, making use of density functional theory (DFT) calculations to elucidate the nature of the interaction between the molecule and the metal surface. Of crucial importance in such calculations is the description of the nonbonded van der Waals (vdW) interactions between the adsorbate and the surface. Traditional generalized-gradient approximation (GGA) functionals are widely known to substantially underestimate the adsorption energies of AB, and many other adsorbates, to Ag(111) and Au(111) surfaces, due to their inability to reliably capture the noncovalent contribution to the interaction energy at medium- to long-range interatomic separations [20,29,30].

However, recovering the experimentally determined details of the adsorption of AB at Au/Ag(111) has also proven challenging for a number of DFT functionals, including functionals that incorporate approaches for capturing noncovalent interactions more reliably. Recently, however, a DFT study reported by Maurer *et al.* [27] illustrated how finite temperature effects can play a key role in the binding of azo-benzene at the Ag(111) surface, in this instance at the desorption temperature for this system. The findings from this study strongly suggested that the adsorption energy at 0 K should therefore be greater than the experimentally determined adsorption energy (which is relevant to a temperature of ∼400 K). For instance, the PBE+D2, PBE + vdW^{surf} and PBE + vdW^{TS} functionals all yield adsorption energies at 0 K that are ⩾ 150% of the experimentally reported adsorption energy (determined at ∼400 K) [21,23,25,27]. Currently, one of the most reliable estimates of the adsorption energy of azo-benzene on Ag(111) has been reported for the combination of the Perdew-Burke-Ernzerhof (PBE) functional [31] with the many-body-dispersion (MBD) method [32]. Using this approach, Maurer *et al.* [27] reported excellent agreement between the absolute experimentally observed adsorption energy of ∼1.0 eV (determined at ∼400 K) [23,28] and their simulated absolute adsorption energy, calculated at 400 K, of 0.99 ± 0.17 eV. Moreover, these authors also reported the calculated absolute adsorption energy at 0 K to be 1.24 eV, which is ∼20% greater than the experimentally determined (400 K) value.

In the present study the adsorbed geometries and energies of azobenzene (AB), 2,2′,6,6′-fluoroazobenzene (FAB), and 2,2′,6,6′-tetrachlor-azobenzol (ClAB), both in the gas phase and at the Ag(111) and Au(111) surfaces, have been calculated using the revPBE-vdW-DF exchange-correlation functional [33–35]. The vdW-DF approaches use an explicit nonlocal correlation term to describe the dispersion interactions and have been applied to a wide range of systems [30,36–40]. Previously reported plane-wave density functional theory (PW-DFT) calculations using the revPBE-vdW-DF functional of the adsorption energies of noncovalently adsorbed molecules to noble-metal interfaces have shown good agreement with experiment [40–47]. The adsorption energy of the *trans* isomer of AB (tAB) to Ag(111) has previously been reported, involving calculations using the revPBE-vdW-DF functional [24]. However, in this study the surface-adsorbed form of the *cis* isomer of AB (cAB) was not investigated, and no calculations were reported for the Au(111) surface. Here,
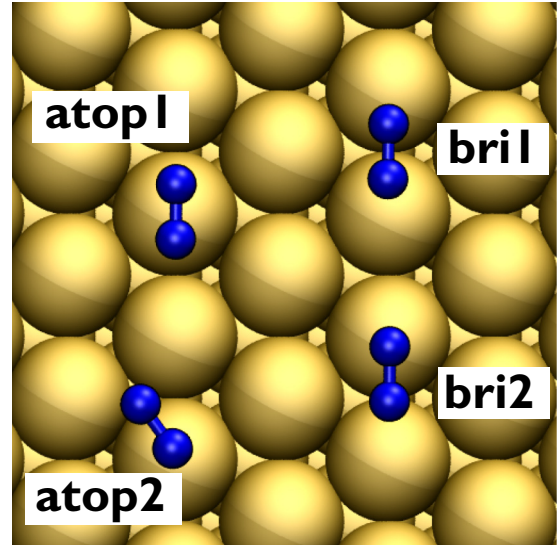

FIG. 1. Initial positions of the N atoms of the AB molecules, for the four initial adsorption sites considered in this work, used to determine the adsorption site of lowest energy. For clarity, only the nitrogen atoms of the AB molecule are shown.

we report the use of revPBE-vdW-DF PW-DFT calculations to predict the structure and properties of AB, FAB, and ClAB in both the *trans* and *cis* forms, both free in the gas phase, and adsorbed at the Au(111) and Ag(111) surfaces. In addition, we have predicted the optical spectra for each isomer of each molecule in the gas phase and adsorbed at both metal surfaces. Our results indicate that there are subtle but important differences in the adsorption of FAB and ClAB that offer promising routes for exploitation in bionanotechnology applications.

II. METHODS

The minimum-energy structure of each isomer (*trans* and *cis*) of AB, FAB, and ClAB was determined for both the gas phase and adsorbed at the Au(111) and Ag(111) interfaces, using geometry optimization, with all atoms allowed to relax. For the interface systems, four different initial structures of the molecule/surface configurations were explored. The four different initial sites are indicated in Fig. 1. After each geometry had been optimized, the total potential energy of the system was then determined from a single point energy calculation. The adsorption energy E_{ads} was calculated using

$$E_{ads} = E_{surf-xAB} - E_{surf} - E_{xAB}, \qquad (1)$$

where $E_{surf-xAB}$ is the energy of the system with the molecule adsorbed to the metal surface with $x = t$ or c (*trans* or *cis*), E_{surf} is the energy of the clean metal surface, and E_{xAB} is the energy of the azobenzene isomer in the vacuum. The relative stability of the *cis* and *trans* isomers, ΔE_{t-c}, in the unadsorbed state was determined using

$$\Delta E_{t-c} = E_{tAB} - E_{cAB}. \qquad (2)$$

Similarly, the relative stability of the *cis* and *trans* isomers, $\Delta E_{\text{surf-t-c}}$, in the adsorbed state was determined using

$$\Delta E_{\text{surf-t-c}} = E_{\text{surf-tAB}} - E_{\text{surf-cAB}}. \quad (3)$$

All PW-DFT calculations were performed using the QUAN-TUM ESPRESSO code, version 5.0.5 [48]. The revPBE-vdW-DF exchange-correlation functional [33,34] and ultrasoft pseu-dopotentials [49] were used throughout. All calculations were performed using cutoffs for the plane-wave kinetic energy and electron densities of 25 and 200 Ry, respectively, and were not spin polarized. The Gaussian smearing method, with a width of 0.05 Ry, was used for Brillouin-zone integration. The SCF calculation convergence threshold was set to 1×10^{-6} Ry for all calculations. For the geometry optimizations a 0.026 eV/Å force convergence criterion was applied; during the single point calculations the forces were checked to ensure the threshold was not exceeded. These cutoffs (and the conversion criteria) are the same as those previously used to determine the adsorption energies of a wide range of molecules to the Au(111) and Ag(111) surfaces [41,42]. We checked the convergence of the adsorption energy with respect to the k-point mesh and plane-wave cutoffs, finding that E_{ads} was converged to within ±0.01 eV.

For the metal surfaces, a Au/Ag slab constructed from a $p(6 \times 4)$ supercell, four atomic layers thick, was used (a total of 96 metal atoms). All systems had periodic boundary con-ditions applied in all three dimensions and were constructed such that along the z axis a distance of at least 10 Å separated the molecule from the periodic image of the slab surface. For the single point energy calculations the distance in the z was increased to ensure that a distance of at least 20 Å separated the molecule from the periodic image of the slab surface. k-point meshes of $2 \times 3 \times 1$ and $4 \times 6 \times 1$ were used for the geometry optimizations and single point calculations, respectively.

The geometries of the molecules were analyzed by consid-ering a range of structural parameters. Internal angles ω and β were designated as the C-N-N-C and C-C-N-N dihedral angles of the AB molecules. For the adsorbed molecules, $d_{\text{N1-Me}}$ and $d_{\text{N2-Me}}$ were defined as the distance between the nitrogen atoms and the metal surface, with the closer nitrogen always assigned as N1. $\tilde{\omega}_1$ and $\tilde{\omega}_2$ were defined as the angle between the plane of the rings and the surface plane, with $\tilde{\omega}_1/\tilde{\omega}_2$ corresponding to the ring attached to N1/N2.

Transition energies and dipoles for the geometries obtained from the PW-DFT calculations were computed using the Q-Chem 4.4 electronic structure program [50] at the density functional theory configuration interaction with singles (CIS) level of theory. The Coulomb attenuated B3LYP (CAM-B3LYP) functional [51] was used together with the 6-31G(d,p) split-valence basis set for all atoms of the organic part. The relatively inexpensive CIS method was chosen because of the large number of the excited states needed to be computed in the case when the metallic surface, represented by a metal cluster (Ag_{20} or Au_{20}), was present. Our benchmarking calculations with time-dependent DFT (response theory) for an isolated system (with no metal surface present) showed a systematic redshift of the excitation energies on the order of 25 nm for n-$\pi*$ peak and 7 nm for π-$\pi*$ peak. Standard Los Alamos effective core potential LANL2DZ [52] and a
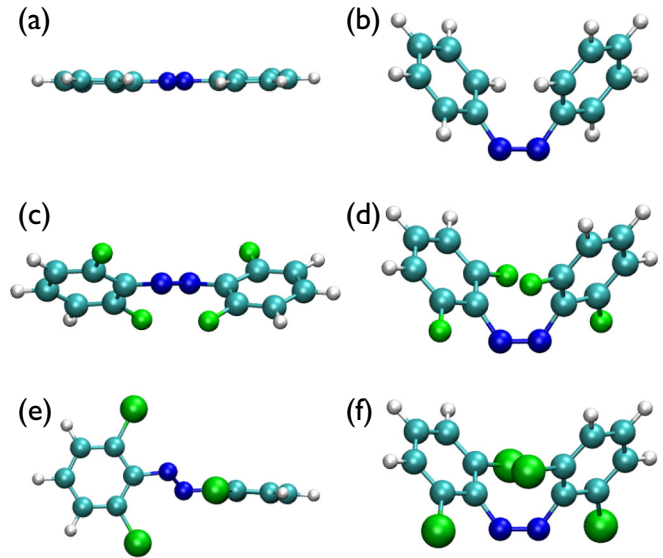

FIG. 2. Minimum-energy structures of (a) *trans* azobenzene, (b) *cis* azobenzene, (c) *trans* fluoro-azobenzene, (d) *cis* fluoro-azobenzene, (e) *trans* chlor-azobenzol, and (f) *cis* chlor-azobenzol in the gas phase.

matching LANL2DZ basis sets for the valence electrons were employed for the description of the metal part component. The extinction spectra of all systems were simulated from the calculated transition dipole moments and excitation energies with the Lorentzian line shape and the full width at half maximum (FWHM) of 0.2 eV, characteristic to small organic molecules. For the molecules in the absence of the metal surface we computed 15 excitations, whereas the systems with the metal present required at least 75 excitations to capture the π-$\pi*$ peaks.

In each case, we took the structure of the molecule predicted from the PW-DFT calculations, and used these frozen geometries to calculate our spectra. In the case of the surface-adsorbed systems, we clipped out the PW-DFT optimized structure of the molecule plus a metal cluster (see below) from the (111) metal slab in the corresponding periodic cell. As mentioned above, out of necessity, we approximated the metal surface *via* the use of a cluster model. Methodologically, truncation of the Ag/Au(111) slab into a smaller cluster model had to comply with two requirements: first, the number of electrons in the system should be adequate relative to the computational resources available, and, second, the spin multiplicity should be kept at unity. A trial-and-error approach revealed an optimal size of the clusters that met these criteria to be 20 atoms, considering the number of excitations we needed to compute to capture the UV part of the spectra. In this instance the 20-atom cluster was configured as two atomic layers thick, with ten atoms per layer.

III. RESULTS

A. Gas-phase geometries

In the gas phase, our revPBE-vdW-DF DFT calculations indicate the *trans* structure of AB to be planar, as shown in Fig. 2. As expected, substitution of the hydrogens at

TABLE I. Adsorption energies, E_{ads} in eV, of the azobenzene molecules at lowest energy sites on the Ag(111) and Au(111) surfaces, and the energy difference between the *cis* and *trans* isomers, $\Delta E_{c \to t}$ in eV, for the different systems.

| Molecule | System | E_{ads} / eV | | | ΔE_{t-c} / eV | |
		trans	*cis*	Expt.	DFT	Expt.
AB	Gas				−0.52	−0.49 ± 0.03[a]
	Au(111)	−1.19	−0.96	−1.00 ± 0.15[b]	−0.75	
	Ag(111)	−1.06	−1.00	−1.02 ± 0.06,[b] −1.00 ± 0.10[c]	−0.58	
FAB	Gas				−0.24	
	Au(111)	−1.25	−0.97		−0.52	
	Ag(111)	−1.11	−1.08		−0.27	
ClAB	Gas				−0.28	
	Au(111)	−1.49	−1.14		−0.64	
	Ag(111)	−1.33	−1.10		−0.52	

[a]Ref. [53].
[b]Ref. [28].
[c]Ref. [23].

the *ortho* positions for halogen atoms causes the rings to twist with respect to the central N = N bond. For tFAB the minimum-energy geometry featured the planes of the two rings at ~60° to each other, although this structure was only 0.03 eV lower in energy than a planar geometry. This small energy difference in the two structures might explain why x-ray structures of the molecule in the crystalline form reveal planar molecules [17]. In the case of ClAB, the twisting is more substantial with the minimum-energy structure supporting the two rings approximately orthogonal to each other. In contrast to the differences in the *trans* structures of the three molecules, the *cis* structures are all very similar to each other. The energy difference between the two isomers of AB in the gas phase, given by the revPBE-vdW-DF functional, is −0.52 eV, see Table I, which compares well with the experimental value of −0.49 ± 0.03 eV. For FAB and ClAB the magnitude of this energy difference is approximately halved, to −0.24 and −0.28 eV, respectively.

TABLE II. Adsorption energies, E_{ads} in eV, of the azobenzene molecules at the different sites on the Ag(111) and Au(111) surfaces.

| Molecule | Surface | E_{ads} / eV | | | |
		bri1	bri2	atop1	atop2
tAB	Au(111)	**−1.19**	−1.17	−1.16	−1.18
	Ag(111)	**−1.06**	−0.99	−0.97	−1.00
tFAB	Au(111)	−1.25	**−1.25**	−1.24	−1.23
	Ag(111)	−1.10	**−1.11**	−1.09	−1.09
tClAB	Au(111)	−1.46	**−1.49**	−1.46	−1.45
	Ag(111)	−1.28	−1.31	−1.30	**−1.33**
cAB	Au(111)	**−0.96**	−0.95	a	a
	Ag(111)	**−1.00**	−0.96	a	−0.93
cFAB	Au(111)	−0.95	**−0.97**	a	a
	Ag(111)	**−1.08**	b	b	−1.02
cClAB	Au(111)	−0.94	**−1.14**	a	a
	Ag(111)	−1.05	**−1.10**	−1.08	c

[a]Goes to bri2.
[b]Goes to bri1.
[c]Goes to atop1.

B. Adsorbed geometries and energies

The adsorption energies of the different isomers/molecules at the different sites on the Ag/Au surfaces are given in Table II. The bri1 site was found to be the lowest energy site for both isomers of AB at both the Ag(111) and Au(111) surface, although in both cases the differences in E_{ads} at the different sites is modest (especially for the *trans* isomer), in agreement with previous reports of the adsorption of AB at Ag(111)/Au(111) surfaces with alternative functionals [20,21]. The substitution of hydrogens for halogen atoms led to an increase in the adsorption strength, with a trend in binding strength of ClAB > FAB > AB, although in some cases the increase in energy was modest. With the exception of cFAB@Ag(111), the lowest energy site was found to no longer be the bri1 site. Instead, the bri2 site, or in the case of tClAB@Ag(111) the atop2 site, was favored. However, the energy differences between sites was still typically ⩽ 0.06 eV, less than the difference in E_{ads} of the two isomers at a surface and less than the difference in E_{ads} for the *trans* isomer at the two metal interfaces.

The adsorption energies for the three molecules at the Au(111) and Ag(111) interfaces at the lowest energy sites are summarized in Table I. For AB the calculated adsorption energies agreed well with the experimentally determined energies obtained from TPD [23,28]. These previously reported experimental data indicated that adsorption of AB to the two metal interfaces was essentially isoenergetic. Here, our revPBE-vdW-DF calculations indicate that tAB adsorption was slightly more favorable at Au(111) relative to Ag(111), while adsorption of cAB was found to be stronger at Ag(111) than Au(111). However, the energy difference for the *cis* isomers at the two metals was only 0.04 eV. For all three molecules, the difference in E_{ads} for the two isomers was greater at the Au(111) interface than at the Ag(111) interface, and likewise, ΔE_{t-c} was always greater at the Au(111) interface. For AB and FAB, ΔE_{t-c} at the Ag(111) surface was approximately equal to that in the gas phase, and was found to be ~0.25 eV lower than that at the Au(111) surface. Moreover, the significant reduction in ΔE_{t-c} for FAB compared to AB is carried over to both surfaces. In contrast, when adsorbed at

TABLE III. Geometrical parameters of the isomers of the azobenzene molecules adsorbed and in the gas phase. See text for definitions of these parameters.

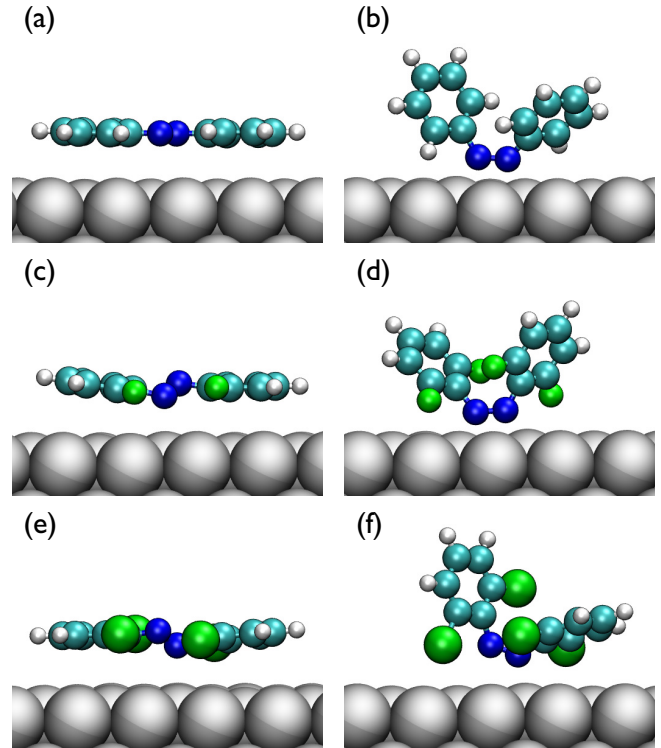| Molecule	System	$d_{\text{N1-Me}}$/Å	$d_{\text{N2-Me}}$/Å	ω/°	$\tilde{\omega}_1$/°	$\tilde{\omega}_2$/°	β/°
tAB	Gas			179.6			2.9
	Au(111)	3.57	3.57	179.5	1.2	1.1	0.6
	Ag(111)	3.53	3.54	178.7	1.8	1.2	0.8
tFAB	Gas			173.9			30.3
	Au(111)	3.38	3.80	178.6	3.2	1.0	28.4
	Ag(111)	3.14	3.69	175.9	8.2	1.6	34.4
tClAB	Gas			172.5			46.7
	Au(111)	3.40	3.94	179.9	2.4	2.2	38.7
	Ag(111)	3.29	3.94	176.9	6.9	1.5	42.9
cAB	Gas			10.4			48.5
	Au(111)	2.47	2.76	14.6	21.0	91.2	40.1
	Ag(111)	2.37	2.45	20.3	37.9	105.9	39.9
cFAB	Gas			10.3			57.3
	Au(111)	2.83	3.27	11.6	10.3	81.5	50.8
	Ag(111)	2.37	2.46	21.4	58.4	131.5	50.4
cClAB	Gas			6.5			59.3
	Au(111)	3.27	3.86	7.4	3.1	76.4	55.2
	Ag(111)	2.91	3.32	12.4	17.6	95.1	55.2

FIG. 3. Minimum-energy structures of (a) *trans* azobenzene, (b) *cis* azobenzene, (c) *trans* fluoro-azobenzene, (d) *cis* fluoro-azobenzene, (e) *trans* chlor-azobenzol, and (f) *cis* chlor-azobenzol adsorbed at the Ag(111) surface.

either metal surface, ClAB showed only a minor reduction in ΔE_{t-c} compared with AB. This lack of reduction is especially pronounced for the Ag(111) surface, where the ΔE_{t-c} of ClAB showed a significant increase compared to the gas phase value, unlike that of AB and FAB.

Table III provides the geometric parameters for the minimum energy structures of each molecule when adsorbed at the metal surface and in the gas phase. Figure 3 shows the adsorbed structures at the Ag(111) interface. The structures at the Au(111) (not shown) were found to be very similar to the corresponding Ag(111)-adsorbed structures. tAB adsorbed to both metal surfaces in a planar geometry, with the nitrogen atoms predicted to be located ∼3.5 Å above the metal surface,

as compared with the experimental value of 2.97 ± 0.05 Å. This discrepancy with the experimental values of $d_{\text{N-Me}}$ is not unexpected; overestimation of the separation distances of surface-adsorbed molecules is a known limitation of the revPBE-vdW-DF functional [29,30].

Table IV provides a summary of the geometric parameters, $d_{\text{N-Me}}$ and ω, obtained for AB adsorbed at the Au(111) and Ag(111) interfaces from previous DFT calculations at 0 K,

TABLE IV. A summary of the literature values of $d_{\text{N-Me}}$ and ω of the isomers of azobenzene adsorbed at the metal interfaces obtained from previously reported DFT calculations, along with the current work.

		$d_{\text{N-Me}}$[a]/Å				ω/°			
		tAB		cAB		tAB		cAB	
Reference	Functional	Au(111)	Ag(111)	Au(111)	Ag(111)	Au(111)	Ag(111)	Au(111)	Ag(111)
Present work	revPBE-vdW-DF	3.57	3.54	2.62	2.41	179.5	178.7	14.6	20.3
20	PBE	3.50	3.64	2.31	2.27	180	180	18	23
21	OBS	3.48	3.60	2.24	2.20	180	180	19	25
21	PBE + D2		2.75		2.14		180		25
21	PBE + vdW$^{\text{TS}}$	3.28	2.98	2.23	2.16	180	179	18	25
24	revPBE-vdW-DF		3.57						
24	optB86b-vdW-DF		2.85						
25	PBE + vdW$^{\text{TS}}$		2.95				178.2		
25	PBE + vdW$^{\text{surf}}$		2.61				175.5		
26	PBE + vdW$^{\text{surf}}$	3.13	2.58						
27	PBE + vdW$^{\text{surf}}$		2.78						
27	PBE + MBD		2.60						

[a]The distance between the center of mass of the two N atoms and the metal surface.

compared with the results of the current work. Many previous calculations did not report separate values for $d_{\text{N1-Me}}$ and $d_{\text{N2-Me}}$, therefore $d_{\text{N-Me}}$ (the adsorption height) describes the distance between the center of the mass of the two nitrogen atoms and the metal surface. As expected, the adsorption height for the revPBE-vdW-DF functional is towards the upper end of the range of calculated values, for both the *cis* and *trans* states and on both metal surfaces. However, the discrepancy of the revPBE-vdW-DF adsorption height with previous $PBE + vdW^{TS}$ and $PBE + vdW^{surf}$ calculations appears particularly pronounced for the *trans* state adsorbed on Ag(111), and is less severe for the *trans* state adsorbed on Au(111), and also the *cis* state adsorbed on both metal surfaces.

Furthermore, as illustrated in Table IV, in all previous studies where data were reported for both tAB and cAB, the adsorption height was smaller for cAB than for tAB, typically by ~ 1 Å. In addition, the adsorption height of cAB on Ag(111) was always smaller than that of cAB adsorbed on Au(111), although in some cases this difference was negligible (<0.1 Å). In contrast, the relative difference in the adsorption heights of tAB to the two metal surfaces was found to differ depending on the functional used. For example, PBE and OBS calculations predicted tAB to adsorb closer to the Au(111) interface, while $PBE + vdW^{TS}$, $PBE + vdW^{surf}$, and revPBE-vdW-DF (albeit with a narrow margin) predicted the opposite. All functionals predicted that AB adsorbed in a conformation which had undergone only minor distortion relative to the gas phase structure [21,23]. All DFT calculations indicated that, at 0 K and low coverage, tAB absorbs in an essentially planar conformation ($\omega = 180°$), in agreement with experimental observations [23,25]. There is also good general agreement for ω for cAB, with a consistently lower value found for the molecule adsorbed on Au(111) relative to the Ag(111) across a range of functionals. The value for β was not mentioned in several previous studies, but was reported as 0.6 and 2.0° for tAB@Ag(111) using the $PBE + vdW^{TS}$ and $PBE + vdW^{surf}$ functionals, respectively [25], which is consistent with the value of 0.8° obtained in the present work.

Despite the gas phase structures of tFAB and, especially, tClAB, featuring the phenyl rings out of plane with each other, on both metal surfaces the rings were found to be essentially coplanar [see Figs. 3(c)–3(f)]. In the case of tAB the two central nitrogen atoms were located equidistant from the surface, while for the halo-ABs one nitrogen is located closer to the surface than the other. To elaborate, in the latter case, the two rings were approximately coplanar and lay almost parallel to the surface plane, but the central $N = N$ bridge was oriented out of the plane defined by the rings. The separation distance was greater on Au(111) than on Ag(111), and greater for tFAB than for tClAB, but in general these distances were found to be very similar. For all three species, $d_{\text{N-Me}}$ was predicted to be smaller for the *cis* isomer than for the *trans* isomer, suggesting an enhanced N-metal interaction for the *cis* isomer. This might explain why, despite the greater contact surface area (between molecule and surface) of the *trans* form, the difference in E_{ads} for the two isomers is not as substantial based on these arguments alone. Specifically, we suggest that the reduction in the interaction between the phenyl ring(s) and the metal surface for the *cis* form is compensated by this enhanced N-metal interaction. Likewise, the reduced difference in E_{ads} between

the two isomers at the Ag(111) surface could be explained by the decrease in $d_{\text{N-Me}}$ on the two metals, which was greater for Ag(111) than for Au(111). In addition, $\tilde{\omega}_1$ was always smaller at Au(111) than at Ag(111), indicating that at the Au(111) surface, there is a stronger preference to orient one of the rings more parallel to the metal surface plane. The larger spatial extent of Cl may also hinder the close N-metal interaction, which in turn may allow the phenyl ring attached to N1 to play a greater role in the adsorption, resulting in a smaller $\tilde{\omega}_1$ than was noted for either cAB or cFAB.

C. Spectra

The calculated spectra for all three molecules are summarized in Fig. 4. Here, we compare the spectra for each of the three molecules (in the *trans* and *cis* isomerization states), obtained for three cases: (1) the unadsorbed molecule in the gas phase geometry (denoted "gas"), (2) the unabsorbed molecule in the surface-adsorbed geometry (denoted "Au/Ag free"), and (3) the surface-adsorbed molecule. We reiterate here that our spectra for the surface adsorbed states, namely case (3) as summarized above, were, by necessity, calculated using a cluster model of the Ag/Au(111) surface.

It is well established that the planar geometry of unsubstituted gas phase trans-isomer of AB results in a (counterintuitive) substantial spatial overlap of nitrogen lone pair n orbitals [54]. Consequently, the through-space interaction between n orbitals results in the stabilized antisymmetric combination of these orbitals, which, in turn, leads to the symmetry forbidden n-π^* transition [54]. Substituting ortho-hydrogens with heavier and larger F and Cl atoms results in distorted planarity with an inter-ring twist, somewhat similar to *cis* conformation. The n-π^* transition became allowed because of the broken symmetry of the n-orbital combination. In addition, this resulted in destabilization of π^* orbital, which is evidenced by a blueshift in the spectral position of the π-π^* peak. Analysis of the gas phase spectra of F- and Cl-substituted cis-azo-benzenes showed a redshift of the n-π^* peak, consistent with an increase of the inter-ring dihedral angle from 30° to 47°, respectively. This redshift can be explained by destabilization of molecular n orbital due to the weakened through-space interaction between the nitrogen lone pair orbitals. Adsorption on a metal surface restored planarity of the FAB and ClAB *trans* isomers. Consequently, the n-π^* becomes forbidden. For *cis* isomer the redshift of n-π^* peak was still observed.

To summarize, two factors greatly affect UV-visible absorption spectra of the studied compounds, that is: the effect of halogen substitution in the ortho position and the effect of adsorption on the metal surface (which for our spectral calculations was approximated by a metal cluster). The latter is characterized by relative stabilization of the π^* orbital for both cis- and trans-isomers, as evidenced by the redshift (approximately 15 nm) of the spectral position of the π-π^* peak, and the relative destabilization of the n orbital for the cis-isomer, as indicated by a larger (approximately 50 nm) redshift of the spectral position of the n-π^* peak. Stabilization of the π^* orbital can be associated with a slight increase of conjugation through the $N = N$ bond in the metal-adsorbed geometry, whereas de-stabilization of the n orbital is likely to
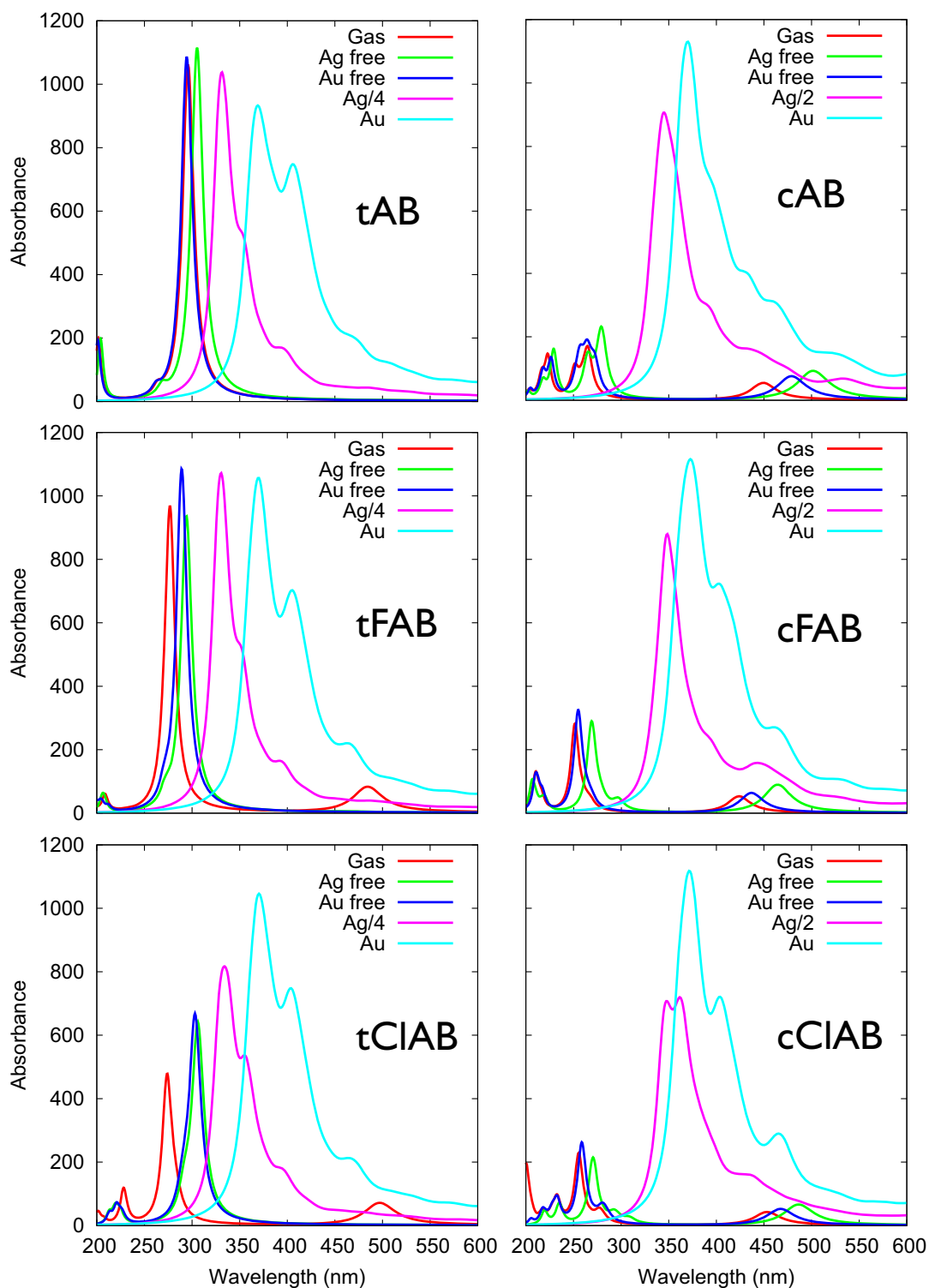
FIG. 4. Calculated spectra for AB, FAB, and ClAB in the *trans* and *cis* isomers. "Gas" denotes the free molecule in the gas phase geometry, "Ag/Au-free" denotes the free molecule in the surface-adsorbed geometry, and "Ag/Au" denotes the surface-adsorbed molecule. Peak heights have been scaled for Ag-adsorbed cases as indicated in the figure legend.

be a consequence of the increased dihedral angle between the aryl rings (approximately $10°$ for the unsubstituted gas phase geometry vs approximately $20°$ for unsubstituted adsorbed geometries), which results in a lesser spatial overlap between nitrogen lone pair orbitals. Additionally, as mentioned above, adsorption on the metal surface restores planarity of the

ortho-halogen-substituted trans-isomers, which results in reinstatement of the n-$\pi*$ peak. The effect of halogen substitution is also twofold: first, planarity of substituted trans-isomers becomes distorted in accord with the size of the halogen atom (the effect is more pronounced for Cl than for F), and, second, the electron density around N $=$ N bond is reduced in accord
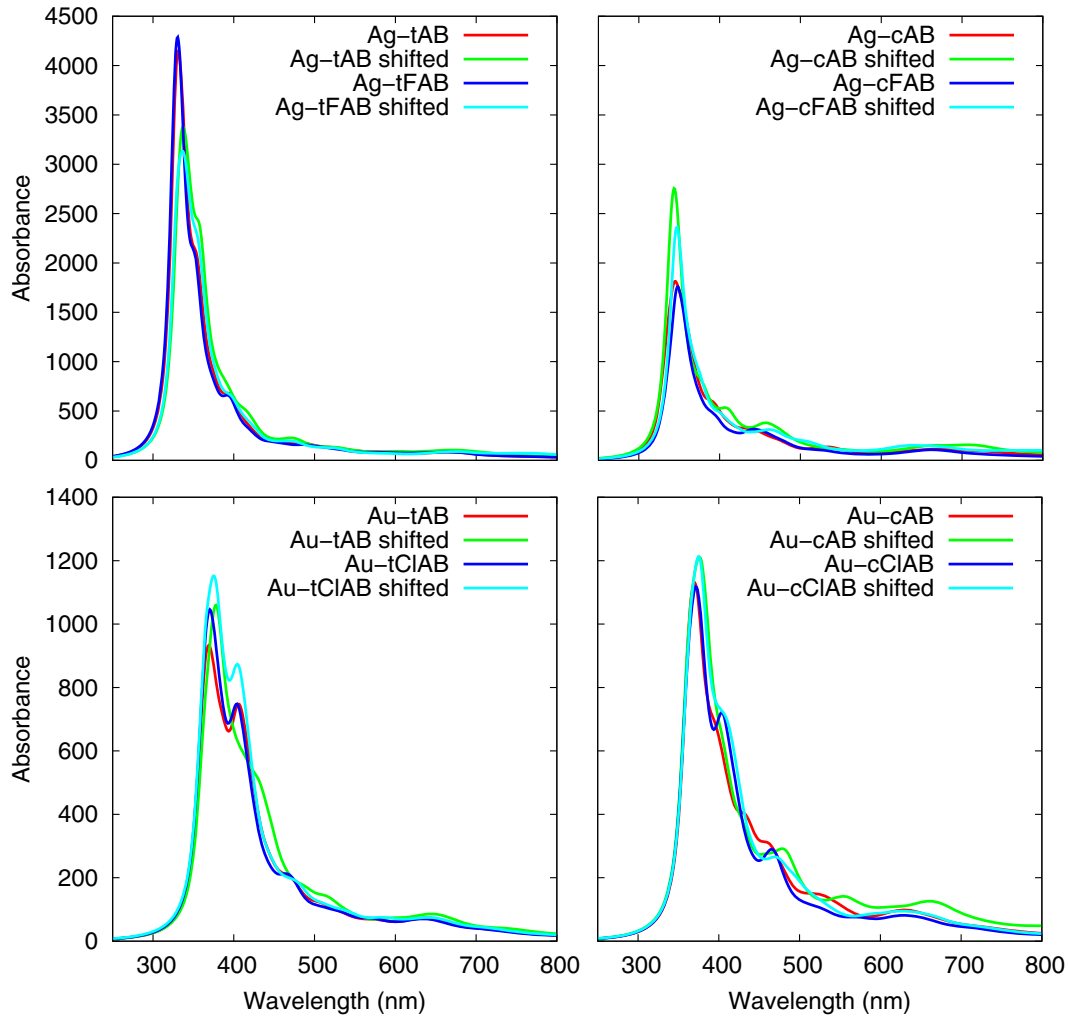
FIG. 5. Comparison of calculated exemplar spectra for the *trans* and *cis* isomers of AB, FAB, and ClAB adsorbed on the metal cluster surface, both for the original adsorption height, and where the surface-molecule distance has been reduced by 0.5 Å, denoted "shifted."

with the electronegativity of the halogen substituent (which will be greater for F than for Cl) [16]. The former results in a relative redshift of the n-π^* peak (destabilization of the n orbital), whereas the latter results in a blueshift, relative to the unsubstituted cis-isomer, of the same peak (stabilization of the n orbital).

To check a possible effect of the overestimation of the adsorption height on UV-visible spectra, we translated the adsorbed molecules by 0.5 Å closer to the Ag and Au cluster surfaces and recalculated the spectra (again without subsequent geometry optimization). Examples of the resulting spectra are presented in Fig. 5. The most pronounced effect we observed was an approximately 7 nm redshift of the π-π^* peak for both unsubstituted and substituted trans-isomers, independent of the metal (Ag or Au) cluster. We suggest this is due to the greater overlap between d orbitals of the metal and the electronic π system of the molecules. The trans-isomers lie almost flat with respect to the cluster surface and the electronic π system is always perpendicular to the planes of both aryl rings, hence, a smaller adsorption height resulted in a greater overlap and stabilization of the molecular π^* orbital. For the unsubstituted and substituted cis-isomers adsorbed on the Ag surface, no significant shifts were observed, whereas

approximately 4-nm shifts were observed for the adsorption on the Au surface. We ascribe this to the fact that one of the aryl rings in the structures adsorbed on Au is almost parallel to the surface, whereas the orientation of both aryl rings is tilted with respect to the Ag surface, hence, the effect of metallic d orbitals overlap with the molecular π system is negligible.

IV. CONCLUSIONS

The effect of halogen substitution at the *ortho* positions of azobenzene (AB) has been investigated both in the gas phase and for molecules adsorbed at Au(111) and Ag(111) surfaces using density functional theory calculations with the revPBE-vdW-DF functional. We considered substitutions with fluorine atoms (FAB) and chlorine atoms (ClAB). Previous studies have indicated that the adsorption energy at 0 K of azo-benzene on Ag(111) should ideally exceed the experimentally determined value observed at finite temperature. Our results obtained using the revPBE-vdW-DF functional provided reasonable comparison with experiment in this respect, and moreover should provide reliable binding trends as identified from our results for the halo-substituted azo-benzenes. In the gas phase, the presence of the halogen atoms caused a twisting

of the rings in the *trans* form, resulting in a reduction the energy difference between the two isomers. However, in the surface-adsorbed state, the *trans* isomers of both FAB and ClAB adopted an approximately planar conformation with the rings lying nearly parallel with the metal surface. The effect of the presence of the halogen atoms on the geometries of the *cis* isomers was comparatively minor, both in the gas phase and when adsorbed. The weaker interactions between the aromatic rings and the metal surface in the *cis* form appeared to be partially compensated by a stronger nitrogen-metal interaction. Nevertheless, for a given molecule adsorbed at a given surface, the binding strength of the *trans* isomer was always found to be greater than that of the *cis* form. Overall, these effects produced an increase in the relative stability of the *cis* isomer in the case of the adsorbed FAB molecule, but for ClAB the energy difference between the adsorbed isomers was similar to that of the parent AB molecule. We ascribed this to the larger atomic radius of Cl relative to hydrogen and fluorine. This suggests that the relatively bulkier Cl atoms could hinder favorable interactions of the nitrogen sites with the metal surface in the *cis* state. Substitution with the halogen atoms also affected the absorption spectra of the molecules, with the twisting of the *trans* isomer in the halo-substituted species in the gas phase resulting in a peak appearing at ~ 500 nm, due to the $n\text{-}\pi*$ transition no longer being forbidden. This peak is lost for the adsorbed *trans* molecules due to the planarity of the molecules when adsorbed. Our work highlights that even relatively minor modifications to azobenzene can result in distinct differences in how the molecule adsorbs to noble-metal interfaces, opening up possibilities to develop molecular switches with different surface-dependent features.

[1] R. Klajn, J. F. Stoddart, and B. A. Grzybowski, Chem. Soc. Rev. **39**, 2203 (2010).

[2] R. Pardo, M. Zayat, and D. Levy, Chem. Soc. Rev. **40**, 672 (2011).

[3] J. M. Abendroth, O. S. Bushuyev, P. S. Weiss, and C. J. Barrett, ACS Nano **9**, 7746 (2015).

[4] S. Kawata and Y. Kawata, Chem. Rev. **100**, 1777 (2000).

[5] Y. Yu, M. Nakano, and T. Ikeda, Nature (London) **425**, 145 (2003).

[6] D. Bléger, Z. Yu, and S. Hecht, Chem. Commun. **47**, 12260 (2011).

[7] M. Dong, A. Babalhavaeji, S. Samanta, A. A. Beharry, and G. A. Woolley, Acc. Chem. Res. **48**, 2662 (2015).

[8] R. J. Mart and R. K. Allemann, Chem. Commun. **52**, 12262 (2016).

[9] Z. Tang, C.-K. Lim, J. P. Palafox-Hernandez, K. L. M. Drew, Y. Li, M. T. Swihart, P. N. Prasad, T. R. Walsh, and M. R. Knecht, Nanoscale **7**, 13638 (2015).

[10] J. P. Palafox-Hernandez, C.-K. Lim, Z. Tang, K. L. M. Drew, Z. E. Hughes, Y. Li, M. T. Swihart, P. N. Prasad, M. R. Knecht, and T. R. Walsh, ACS Appl. Mater. Interfaces **8**, 1050 (2016).

[11] C.-K. Lim, X. Li, Y. Li, K. L. M. Drew, J. P. Palafox-Hernandez, Z. Tang, A. Baev, A. N. Kuzmin, M. R. Knecht, T. R. Walsh, M. T. Swihart, H. Ågren, and P. N. Prasad, Nanoscale **8**, 4194 (2016).

[12] B. D. Briggs, J. P. Palafox-Hernandez, Y. Li, C.-K. Lim, T. J. Woehl, N. M. Bedford, S. Seifert, M. T. Swihart, P. N. Prasad, T. R. Walsh, and M. R. Knecht, Phys. Chem. Chem. Phys. **18**, 30845 (2016).

[13] A. A. Beharry, O. Sadovski, and G. A. Woolley, J. Am. Chem. Soc. **133**, 19684 (2011).

[14] S. Samanta, A. A. Beharry, O. Sadovski, T. M. McCormick, A. Babalhavaeji, V. Tropepe, and G. A. Woolley, J. Am. Chem. Soc. **135**, 9777 (2013).

[15] D. Bléger and S. Hecht, Angew. Chem. Int. Ed. Engl. **54**, 11338 (2015).

[16] D. Bléger, J. Schwarz, A. M. Brouwer, and S. Hecht, J. Am. Chem. Soc. **134**, 20597 (2012).

[17] C. Knie, M. Utecht, F. Zhao, H. Kulla, S. Kovalenko, A. M. Brouwer, P. Saalfrank, S. Hecht, and D. Bléger, Chem. Eur. J. **20**, 16492 (2014).

[18] H. F. Qian, T. Tao, Y. N. Feng, and Y. G. Wang, J. Mol. Struct. **1123**, 305 (2016).

[19] Y. Ye, J. Pang, X. Zhou, and J. Huang, Comput. Theor. Chem. **1076**, 17 (2016).

[20] E. McNellis, J. Meyer, A. D. Baghi, and K. Reuter, Phys. Rev. B **80**, 035414 (2009).

[21] E. R. McNellis, J. Meyer, and K. Reuter, Phys. Rev. B **80**, 205414 (2009).

[22] E. R. McNellis, C. Bronner, J. Meyer, M. Weinelt, P. Tegeder, and K. Reuter, Phys. Chem. Chem. Phys. **12**, 6404 (2010).

[23] G. Mercurio, E. R. McNellis, I. Martin, S. Hagen, F. Leyssner, S. Soubatch, J. Meyer, M. Wolf, P. Tegeder, F. S. Tautz, and K. Reuter, Phys. Rev. Lett. **104**, 036102 (2010).

[24] G. Li, I. Tamblyn, V. R. Cooper, H.-J. Gao, and J. B. Neaton, Phys. Rev. B **85**, 121409 (2012).

[25] G. Mercurio, R. J. Maurer, W. Liu, S. Hagen, F. Leyssner, P. Tegeder, J. Meyer, A. Tkatchenko, S. Soubatch, K. Reuter, and F. S. Tautz, Phys. Rev. B **88**, 035421 (2013).

[26] R. J. Maurer, V. G. Ruiz, and J. Camarillo-Cisneros, Prog. Surf. Sci. **91**, 72 (2016).

[27] R. J. Maurer, W. Liu, I. Poltavsky, T. Stecher, H. Oberhofer, K. Reuter, and A. Tkatchenko, Phys. Rev. Lett. **116**, 146101 (2016).

[28] M. Schulze, C. Bronner, and P. Tegeder, J. Phys.: Condens. Matter **26**, 355004 (2014).

[29] J. Klimeš and A. Michaelides, J. Chem. Phys. **137**, 120901 (2012).

[30] K. Berland, V. R. Cooper, K. Lee, E. Schröder, T. Thonhauser, P. Hyldgaard, and B. I. Lundqvist, Rep. Prog. Phys. **78**, 066501 (2015).

[31] J. P. Perdew, K. Burke, and M. Ernzerhof, Phys. Rev. Lett. **77**, 3865 (1996).

[32] A. Tkatchenko, R. A. DiStasio, R. Car, and M. Scheffler, Phys. Rev. Lett. **108**, 236402 (2012).

[33] Y. Zhang and W. Yang, Phys. Rev. Lett. **80**, 890 (1998).

[34] M. Dion, H. Rydberg, E. Schröder, D. C. Langreth, and B. I. Lundqvist, Phys. Rev. Lett. **92**, 246401 (2004).

[35] T. Thonhauser, V. R. Cooper, S. Li, A. Puzder, P. Hyldgaard, and D. C. Langreth, Phys. Rev. B **76**, 125112 (2007).

[36] K. Lee, É. D. Murray, L. Kong, B. I. Lundqvist, and D. C. Langreth, Phys. Rev. B **82**, 081101 (2010).

[37] J. Carrasco, B. Santra, J. Klimeš, and A. Michaelides, Phys. Rev. Lett. **106**, 026101 (2011).

[38] G. Graziano, J. Klimeš, F. Fernandez-Alonso, and A. Michaelides, J. Phys.: Condens. Matter **24**, 424216 (2012).

[39] D. J. Carter and A. L. Rohl, J. Chem. Theory Comput. **10**, 3423 (2014).

[40] Z. E. Hughes and T. R. Walsh, Phys. Chem. Chem. Phys. **18**, 17525 (2016).

[41] L. B. Wright, P. M. Rodger, S. Corni, and T. R. Walsh, J. Chem. Theory Comput. **9**, 1616 (2013).

[42] Z. E. Hughes, L. B. Wright, and T. R. Walsh, Langmuir **29**, 13217 (2013).

[43] J. Björk and S. Stafström, ChemPhysChem **15**, 2851 (2014).

[44] J. Carrasco, W. Liu, A. Michaelides, and A. Tkatchenko, J. Chem. Phys. **140**, 084704 (2014).

[45] D. J. Carter and A. L. Rohl, J. Comput. Chem. **35**, 2263 (2014).

[46] M. Rosa, S. Corni, and R. Di Felice, Phys. Rev. B **90**, 125448 (2014).

[47] W. Liu, F. Maaß, M. Willenbockel, C. Bronner, M. Schulze, S. Soubatch, F. S. Tautz, P. Tegeder, and A. Tkatchenko, Phys. Rev. Lett. **115**, 036104 (2015).

[48] P. Giannozzi, S. Baroni, N. Bonini, M. Calandra, R. Car, C. Cavazzoni, D. Ceresoli, G. L. Chiarotti, M. Cococcioni, I. Dabo, A. D. Corso, S. de Gironcoli, S. Fabris, G. Fratesi, R. Gebauer, U. Gerstmann, C. Gougoussis, A. Kokalj, M. Lazzeri, L. Martin-Samos *et al.*, J. Phys.: Condens. Matter **21**, 395502 (2009).

[49] D. Vanderbilt, Phys. Rev. B **41**, 7892 (1990).

[50] Y. Shao, Z. Gan, E. Epifanovsky, A. T. B. Gilbert, M. Wormit, J. Kussmann, A. W. Lange, A. Behn, J. Deng, X. Feng, D. Ghosh, M. Goldey, P. R. Horn, L. D. Jacobson, I. Kaliman, R. Z. Khaliullin, T. Ku, A. Landau, J. Liu, E. I. Proynov *et al.*, Mol. Phys. **113**, 184 (2015).

[51] T. Yanai, D. P. Tew, and N. C. Handy, Chem. Phys. Lett. **393**, 51 (2004).

[52] P. J. Hay and W. R. Wadt, J. Chem. Phys. **82**, 299 (1985).

[53] H. K. Cammenga, V. N. Emel'yanenko, and S. P. Verevkin, Ind. Eng. Chem. Res. **48**, 10120 (2009).

[54] R. Hoffmann, Acc. Chem. Res. **4**, 1 (1971).